ELSEVIER

PII: S0016-2361(97)00093-8

Fuel Vol. 76, No. 10, pp. 919–929, 1997

Printed in Great Britain
0016-2361/97 $17.00+0.00

Flue gas recirculation in a gas-fired laboratory furnace: measurements and modelling

João Baltasar, Maria G. Carvalho, Pedro Coelho and Mário Costa*

Mechanical Engineering Department, Instituto Superior Técnico/Technical University of Lisbon, Av. Rovisco Pais, 1096 Lisboa Codex, Portugal

(Received 22 January 1997)

This paper presents an experimental and numerical study of the effect of flue gas recirculation (FGR) on flame characteristics and pollutant emissions. The experimental study was performed in a small-scale laboratory furnace fired by a gas swirl burner of industrial type. The data reported include simultaneous flue gas concentrations of O_2, CO, CO_2, unburnt hydrocarbons (UHC) and NO_x. In addition, detailed in-flame data for major gas-phase species concentrations and gas temperatures were obtained in the near-burner region for two representative operating conditions. For these conditions, a mathematical model based on the numerical solution of the equations governing conservation of mass, momentum and energy and the transport equations for scalar quantities was used. The flue gas data show a marked decrease of NO_x emissions with FGR without significant effects on flame stability, overall combustion efficiency and CO and UHC emissions. The transition between yellow and blue flame occurs at higher FGR rates as the excess air increases. The detailed in-flame data suggest that prompt NO_x is an important mechanism of NO_x formation for the present flow configuration without FGR and that FGR is an effective method for reducing it. These trends are correctly predicted by the mathematical model. However, discrepancies between the predicted and measured temperature and species concentrations, including NO_x, were found, especially close to the burner. These may be due to the shortcomings of the turbulence model in the prediction of swirling flows. © *1997 Elsevier Science Ltd.*

(Keywords: flue gas recirculation; nitrogen oxides; gas combustion)

One of the most widely used methods of reducing NO_x emission from combustion is flue gas recirculation (FGR). However, FGR seems to have a potential disadvantage regarding flame stability, combustion efficiency and emissions of CO, unburnt hydrocarbons (UHC) and solids[1]. The present work was undertaken to investigate more thoroughly the effects of FGR on flame stability, combustor performance and pollutant emissions. Combustion tests were performed in a relatively small-scale laboratory furnace which allowed collection of reliable and detailed data while representing to some extent the combustion behaviour in full-scale equipment.

Previous related studies[1–5] have concentrated primarily on the influence of FGR on flame stability and NO_x emissions and have yielded a number of useful conclusions. The literature reveals however that most studies on FGR have paid little or no attention to its consequences for CO and UHC emissions. In addition, the lack of detailed in-flame data in most of the available studies prevents a full understanding of several elementary features of the use of FGR in combustion systems.

The present paper reports flue gas concentrations of O_2, CO, CO_2, UHC and NO_x for 24 experimental flames. Together the data allow an assessment of the effect of FGR on flame stability and flue gas emissions at three excess air levels. In addition, detailed in-flame data for major gas-phase species concentrations (including NO_x) and gas temperatures are also reported for two representative conditions, one without and the other with FGR. A parallel mathematical modelling exercise is also summarized and comparisons of the predictions with the in-flame data for the two flames are reported.

* Author to whom correspondence should be addressed. Tel. +351-1-8417378; fax +351-1-8475545

EXPERIMENTAL

Test furnace

A schematic of the experimental facility is shown in *Figure 1*. It comprises a small-scale laboratory furnace up-fired by an industry-type swirl burner equipped with facilities for flue gas recycling. The combustion chamber is cylindrical and consists of five interchangeable steel segments each 0.2 m high and 0.3 m i.d. One of the segments has four rectangular ports for probing and viewing which are closed with quartz or steel inserts. The burner geometry, shown in *Figure 2*, is typical of that used in power stations for wall-fired boilers and consists of a burner gun (i.d. 8 mm, o.d. 12 mm) and a secondary air supply in a conventional double-concentric configuration terminating in a quarl of half-angle 24° and a length/diameter ratio of 1.

Commercial propane (99.8% purity) stored in standard bottles was used. The fuel flow rate was controlled with a

pressure regulator and a valve, and measured using a calibrated rotameter. The secondary air was supplied by an air compressor. The air flow rate was measured using a calibrated rotameter. Before entering the burner the air flowed through an ejector so as to aspirate flue gas directly from the exhaust duct of the furnace as illustrated in *Figure 1*. The remainder of the flue gas was exhausted from the test furnace. The flue gas withdrawn for recirculation was cooled by a water coil placed in the recycling duct, after which the condensate was removed. The flow rate of the recirculated flue gas was controlled by a valve. The oxidant mixture (fresh air+flue gas) was then directed to the burner. A probe was permanently placed just before the burner to measure the oxidant composition so that recirculation rates could be calculated.

Measuring techniques and experimental uncertainties

Flue gas measurements. The sampling of flue gas for the measurement of O_2, CO, CO_2, UHC and NO_x concentrations was achieved using an aerodynamically quenched quartz probe. The probe design and dimensions were similar to those used by Drake *et al.*[6]. The probe was mounted on a traverse mechanism which allowed radial movement across the entire furnace at the exit sampling location ($x/D = 25.7$).

A schematic of the gas analysis system is also shown in *Figure 1*. The gas sample was drawn through the probe and part of the system by a 100% oil-free diaphragm pump. A condenser removed the main particulate burden and condensate. A filter and a dryer removed any residual moisture and particles so that a constant supply of clean dry combustion gases was delivered to each instrument through a manifold to give species concentrations on a dry basis. The analytical instrumentation included a magnetic pressure analyser for O_2 measurements, non-dispersive infrared gas analysers for CO, CO_2 and NO_x measurements and a flame ionization detector for UHC measurements. Zero and span calibrations with standard mixtures were performed before and after each measurement session.

At the furnace exit, radial traverses showed that the concentrations of the species were uniform so that probe effects were likely to be negligible and errors arose mainly from quenching of chemical reactions, sample handling and analysis. Fast quenching of the chemical reactions was achieved and best estimates indicated that the uncertainty due to the solubility of CO_2, UHC and NO_2 in water was negligible. The error due to dissolution was estimated by operating the sampling system with the probe supplied with samples of standard mixtures with compositions similar to those in the flames studied. Reproducibility of the data was within 5% on average.

In-flame measurements. Concentration measurements of O_2, CO, CO_2, UHC and NO_x in the near-burner region were made on a dry basis as described above. However, a water-cooled probe was used instead of the quartz probe. It comprised a centrally located 2 mm i.d. tube through which quenched samples were evacuated, surrounded by two concentric tubes for probe cooling. In the near-burner region the

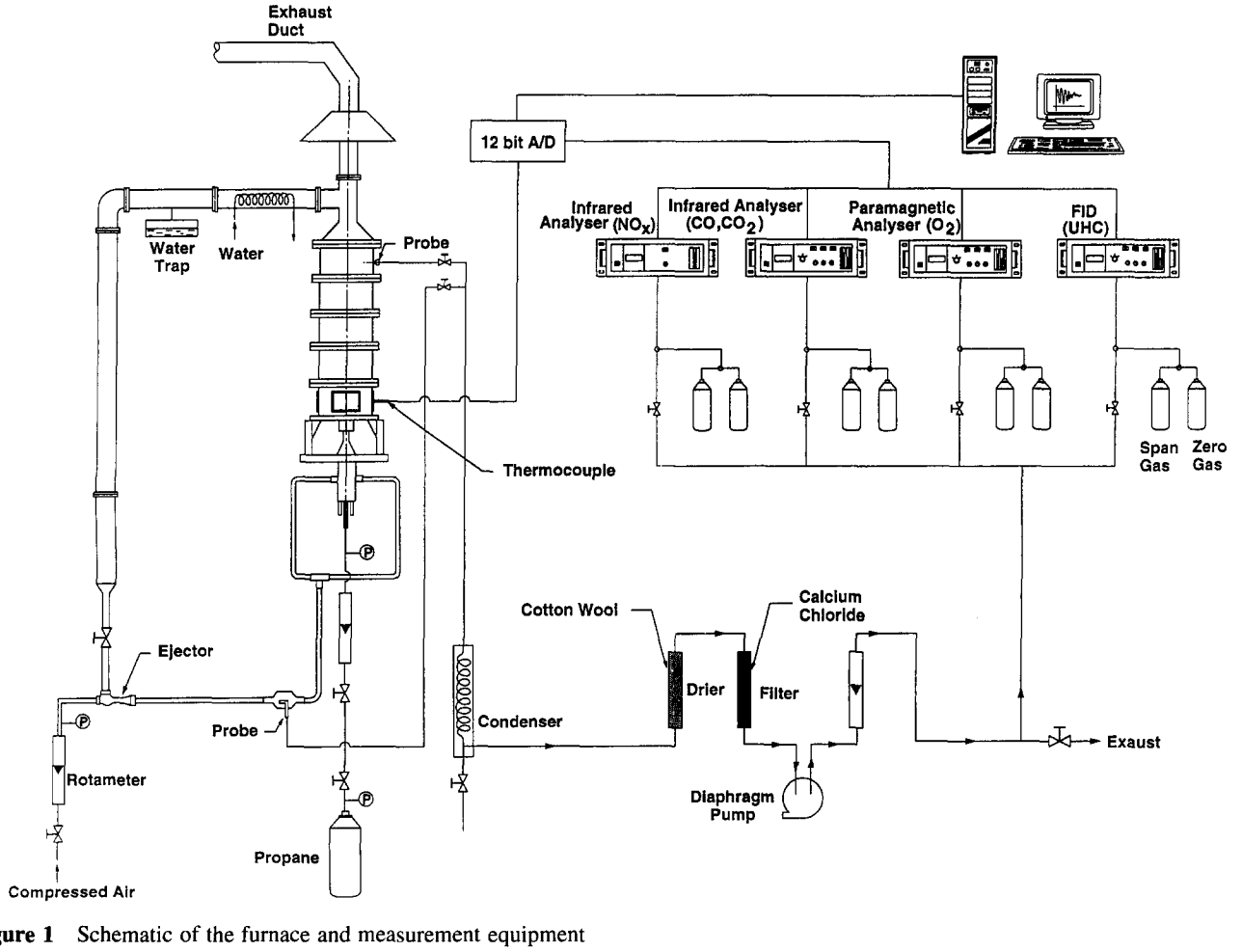

Figure 1 Schematic of the furnace and measurement equipment

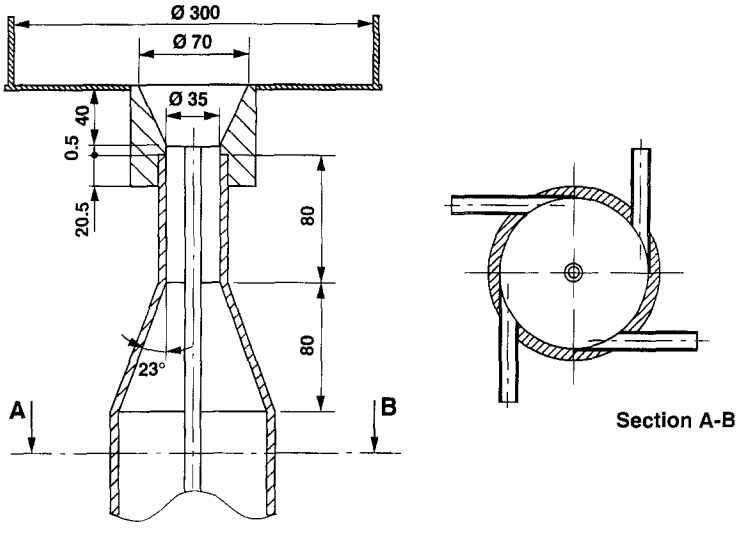

Figure 2 Schematic of the burner arrangement

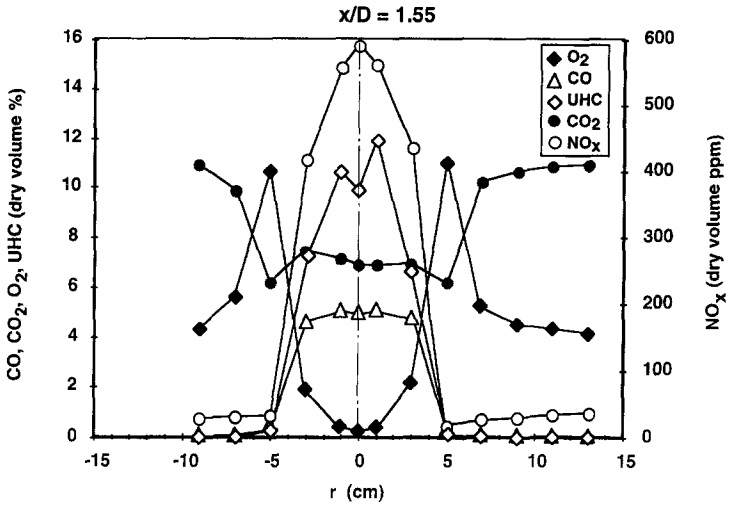

Figure 3 Typical profiles of mean gas species concentration for flame B1 to illustrate flow symmetry

major sources of uncertainties were associated with the quenching of chemical reactions and aerodynamic disturbance of the flow. Fast quenching of the chemical reactions was achieved and the uncertainty due to the solubility of CO_2, UHC and NO_2 in water was negligible. No attempt was made to quantify the probe flow disturbances. The repeatability of the data was within 10% on average.

Gas temperatures were measured using uncoated 25 μm diameter Pt/Pt–13%Rh thermocouples. The hot junction was installed and supported on 300 μm wires of the same material as that of the junction. The 300 μm diameter wires were located in a twin-bore alumina sheath of 4 mm o.d. and placed inside a stainless steel tube. As flame stabilization on the probe was not observed, interference effects were unlikely to have been important and hence no effort was made to quantify them. Radiation losses represent the major source of uncertainty in the mean temperature measurements. An attempt made to quantify them on the basis of a theoretical expression[7] led to uncertainties of ~5% in the regions of highest temperature, and lower elsewhere.

Both probes were mounted on a 3D traverse mechanism, controlled by computer, which allowed axial and radial movements throughout the furnace. The analogue output of the analysers and of the thermocouple was transmitted via A–D boards to a computer where the signals were processed and the mean values computed. No thermal distortion of the probes was observed and the positioning of the probes in the furnace was accurate to within ± 0.5 mm.

Experimental conditions

Substantial efforts were made to establish and maintain flow symmetry in the furnace. *Figure 3* shows typical profiles of mean gas species concentration for the whole furnace diameter to indicate the degree of symmetry. Good symmetry is demonstrated, without which the usefulness of the data for the validation of 2D calculations would be questionable. The repeatability of the data was regularly checked during each experimental session and on different days. On average, all the data could be reproduced within 10% of the mean value.

The furnace operating conditions are summarized in

Table 1 Furnace operating conditions[a] and flue gas data

Flame	Oxidant							R (wt%)	Flue gas composition (dry volume)				
	$\dot{m}$ (10^{-3} kg s^{-1})	V (m s^{-1})	Re	λ	O_2 (vol.% dry)	CO_2 (vol.% dry)	Excess O_2 ratio		O_2 (%)	CO (%)	CO_2 (%)	UHC (ppm)	NO_x (ppm)
A1	4.9	4.7	9972	1.01	20.9	0.0	1.01	0.0	0.24	0.76	13.0	884	14.4
A2	5.2	4.9	10442		20.0	0.5		4.5	0.21	0.66	13.0	437	11.9
A3	5.4	5.2	11011		19.0	0.9		9.8	0.30	0.52	13.2	118	11.0
A4	5.6	5.3	11321		18.5	1.3		12.8	0.16	0.64	13.2	120	7.0
A5	5.8	5.5	11716		17.9	1.7		16.5	0.19	0.78	13.2	149	4.3
A6	6.0	5.7	12199		17.2	2.0		21.0	0.17	0.70	13.1	132	2.6
A7	6.1	5.8	12432		16.9	2.3		23.2	0.17	0.73	13.2	179	2.0
A8	6.6	6.3	13328		15.8	3.0		31.7	0.15	0.59	13.2	190	2.1
B1	5.2	5.0	10553	1.07	20.9	0.0	1.07	0.0	1.48	0.0	12.6	27	32.7
B2	5.5	5.3	11202		19.8	0.5	1.07	5.8	1.54	0.0	12.7	6	31.7
B3	5.7	5.4	11475		19.4	0.8	1.08	8.3	1.72	0.0	12.5	6	31.0
B4	5.9	5.6	11893		18.8	1.2	1.08	12.0	1.70	0.0	12.5	8	27.6
B5	6.1	5.8	12321		18.2	1.6	1.08	15.8	1.50	0.0	12.7	8	25.1
B6	6.5	6.2	13141		17.2	2.2	1.09	23.2	1.56	0.0	12.6	7	16.4
B7	6.9	6.6	13981		16.3	2.8	1.10	30.7	1.60	0.0	12.6	5	10.3
B8	7.0	6.6	14145		16.1	3.0	1.10	32.2	1.43	0.0	12.7	6	8.6
C1	5.6	5.3	11271	1.14	20.9	0.0	1.14	0.0	2.82	0.0	11.8	0.0	42.7
C2	5.9	5.7	11944		19.9	0.4	1.15	5.7	2.97	0.0	11.7	0.0	36.0
C3	6.2	5.9	12473		19.2	0.9	1.16	10.1	2.84	0.0	11.8	0.0	31.7
C4	6.4	6.1	12890		18.7	1.2	1.16	13.6	2.96	0.0	11.7	0.0	27.0
C5	6.8	6.5	13840		17.7	1.9	1.18	21.6	3.20	0.0	11.5	0.0	19.9
C6	6.9	6.6	14037		17.5	2.0	1.18	23.3	3.20	0.0	11.6	0.0	20.1
C7	7.2	6.9	14611		16.9	2.6	1.19	28.1	2.86	0.0	11.8	0.0	16.7
C8	7.4	7.4	15013		16.6	2.6	1.20	31.5	3.21	0.0	11.5	0.0	10.3

[a]For all flames: $\dot{m}_f = 3.1 \times 10^{-4}$ kg s^{-1}; $V_f = 3.32$ m s^{-1}; $Re_f = 6047$; $T_f = 20$°C; $T_{ox} = 20$°C; $S_{ox} = 0.5$

Table 1 and encompass 24 experimental flames. Flames A1, B1 and C1 served as the baseline cases for studying the influence of the FGR on flame stability and flue gas emissions at three excess air levels. It should be noted that, for each group of experimental flames, the fresh air flow rate was held constant and the flue gas flow rate gradually increased. In this work the FGR rate is defined as[1]:

$$R = \frac{\dot{m}_{rec}}{\dot{m}_{air} + \dot{m}_f} \times 100 \quad (1)$$

where $\dot{m}_{rec}$ is the mass of recycled flue gas products per unit time.

Detailed in-flame data and numerical predictions are reported for flames B1 and B6.

MATHEMATICAL MODEL

The mathematical model is based on the numerical solution of the time-averaged equations governing conservation of mass, momentum and energy and the transport equations for scalars describing turbulence and combustion.

The standard k–ε eddy viscosity–diffusivity model was used. In spite of wide use of this model in engineering calculations, it is well known that its performance is generally poor in the simulation of confined swirling flows, particularly in the vicinity of the central toroidal recirculation zone[8]. The poor prediction has been attributed to the inadequate assumption of isotropic viscosity and to the modelling assumptions in the ε-equation. Several modifications of the standard k–ε model have been proposed for isothermal flows to overcome these limitations[9–11]. These modifications were tried in the present work, as described in the section In-flame data under Results and discussion.

Combustion was modelled using the conserved scalar–prescribed probability density function approach. This formalism relies on the assumption that the combustion is controlled by mixing rather than kinetic effects, and that the diffusion coefficients of all the chemical species are equal. Therefore, the instantaneous concentrations of the species may be expressed as a function of a single strictly conserved scalar variable, taken as the mixture fraction. The state relations between mass fractions of the species and mixture fraction were derived from a chemical equilibrium code[12]. Complete equilibrium is assumed up to a critical value of the mixture fraction, f_c. Adiabatic mixing of the mixture at f_c and pure fuel is assumed for mixture fractions greater than f_c [13]. The critical value f_c is selected in such a way that the maximum CO mass fraction of the state relation is equal to the maximum measured CO mass fraction. Additional calculations were performed using the state relations from a flamelet model, but these results are not shown here since no improvement of the predictions was obtained. Mean values of the mass fractions were calculated by integration of the instantaneous values, weighted by a clipped Gaussian probability density function, over the mixture fraction range. The probability density function was fully specified by the mean value and variance of the mixture fraction. Transport equations were solved for these two quantities.

In case of an adiabatic flow, the enthalpy is linearly related to the mixture fraction, provided that the heat and mass diffusion coefficients are equal, and the enthalpy equation need not be solved. In the present work, a transport equation for enthalpy was solved to account for radiative heat losses. The temperature was calculated from the enthalpy using well-known thermodynamic relations and the density was obtained using the ideal-gas law. Turbulent fluctuations were accommodated via an assumed shape for the probability density function, as described above for the species.

Radiation was modelled using the discrete ordinates method[14]. In the present work the computational domain could not be rectangular due to the presence of the quarl. The blocked-off region was handled as proposed by Chai *et al.*[15]. The absorption coefficient of the medium, which is required for the solution of the radiative heat transfer equation, was calculated using a weighted sum of grey gases model, extended to account for soot.

A recent comparison of soot formation and oxidation models suitable for incorporation in turbulent reactive flow calculations has shown that presently available models still present shortcomings[16]. In this work two different models were used. One of them consisted of a simple kinetic expression, as proposed by Khan and Greeves[17]. The other was the model of Moss and co-workers[18,19] with the constants tuned for a confined propane flame as reported by Coelho and Carvalho[16]. The model of Magnussen and Hjertager[20] was used to compute the soot oxidation.

The concentration of NO was calculated by a post-processor code which solved a transport equation for the NO mass fraction. Emissions of NO_x from gas firing have two sources: prompt and thermal NO_x. The prompt mechanism involves the reaction of hydrocarbon fragments and molecular nitrogen in the flame and it depends weakly on temperature[21,22]. The formation of thermal NO_x takes place through the extended Zel'dovich mechanism[23]. The NO formation and destruction was modelled using the Zel'dovich mechanism for the thermal NO and an empirical expression similar to that proposed by de Soete[24] for the prompt NO.

The thermal-NO formation rate is given by:

$$\frac{d[NO]_t}{dt} = 2[O]\frac{(k_1 k_2 [O_2][N_2] - k_{-1}k_{-2}[NO]^2)}{k_2[O_2] + k_{-1}[NO]} \quad (2)$$

where k_1, k_2, k_{-1} and k_{-2} are the forward and reverse rate constants of the following reactions, respectively:

$$O + N_2 \rightleftharpoons NO + N$$

$$N + O_2 \rightleftharpoons NO + O$$

The calculation of the oxygen atom concentration was based on the assumption of partial equilibrium of the chain-branching and propagation reactions of the hydrogen–oxygen mechanism[25].

The prompt-NO formation rate is calculated as:

$$\frac{d[NO]_{pr}}{dt} = Cf\frac{M^{1+b}}{\rho^{1+b}}[O_2]^b[N_2][\text{fuel}]\exp(-E_a/RT) \quad (3)$$

where f is a factor dependent on the number of carbon atoms in the hydrocarbon fuel and on the fuel–air equivalence ratio[26]. Two different values were used for the constant C: $1.2 \times 10^7\ s^{-1}$, as originally proposed by de Soete, and $6.4 \times 10^6\ s^{-1}$, as used by Weber *et al.*[27]. The reaction order for O_2, which can take values from 0 to 1, rising with temperature, was taken as $b = 0.5$, as in Weber *et al.*[27]. The activation energy was taken[26] as 178 kJ mol^{-1} for $T < 1920$ K and 303 kJ mol^{-1} for $T > 1920$ K.

The governing equations were discretized using a finite-difference–finite-volume method. The central difference

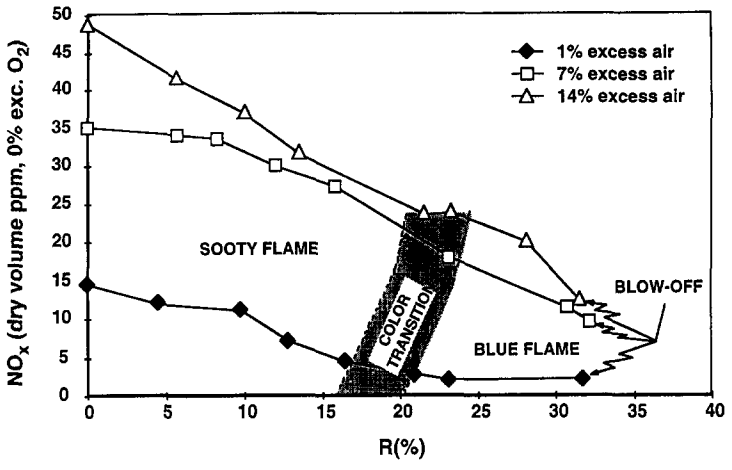

Figure 4 Effect of FGR on NO_x emission at three excess air levels

discretization scheme was used for all the terms except the convective ones, which were discretized using a hybrid central difference–upwind scheme. The discretized equations were solved using the SIMPLE algorithm.

RESULTS AND DISCUSSION

Flue gas measurements

Table 1 summarizes the results of the experiments on the effect of FGR on flue gas emissions. A close examination of the table reveals that increasing R from 0 to ~32% causes the NO_x emissions to decrease throughout the entire range regardless of the excess air level considered. At $\lambda = 1.01$, UHC emissions significantly decrease on increasing R from 0 to 9.8%, beyond which a further increase in R to 31.7% leaves UHC relatively unchanged, while CO emissions appear to be independent of R. At $\lambda = 1.07$, UHC emissions present the same trend as that observed at $\lambda = 1.01$, while CO emissions were not detected for any of the flames. At $\lambda = 1.14$ neither UHC nor CO emissions were detected for any of the flames. Note that the overall combustion efficiency, at a given λ value, remains unchanged as indicated by the CO_2 concentration values.

Figure 4 shows the effect of FGR on NO_x emissions (normalized to 0% O_2 in the combustion products) at the three excess air levels studied and indicates the various combustion regimes observed. It can be observed that blow-off occurs at approximately the same R value regardless of the excess air level. It should be stressed that during furnace operation with recirculating flue gas no flame attachment oscillations were observed and therefore stable combustion* was achieved until blow-off: lifted flames were observed only for R values close to those at which blow-off occurred. It can also be seen in *Figure 4* that the transition between the yellow flame and the blue flame tends to occur at higher values of R as λ increases.

Apart from the limited information available in the literature on the simultaneous effect of FGR on flame stability, combustion efficiency and pollutant emissions, comparison with other work is hindered by the differences in flow configuration and method of flue gas recycling, which may influence the flow aerodynamics.

In-flame data: measurements and modelling

Two of the flames studied above (flames B1 and B6) were chosen for detailed investigation both experimentally and numerically. Radial profiles of measured and predicted temperatures and mole fractions of major gas species, at five axial locations, are shown for flame B1 (without FGR) in *Figures 5 and 6* respectively.

At the station nearest to the burner, combustion is in its initial stages. At the flame axis the temperature is relatively low, which is consistent with the high fuel and CO concentrations and low O_2 concentration. The main reaction zone is located at the flame boundary, as indicated by the temperature peak of ~1200°C at $r \approx 40$ mm. In contrast to the central core of the flame, mixing at the flame boundary is intense due to the shear between the central fuel jet and the oxidant stream. Here the fuel concentration is relatively low, which leads to intense chemical reaction and conversion of CO to CO_2. The rather large peak in O_2 concentration ($r \approx 50$ mm) and the region of depressed temperature ($55 \leq r \leq 65$ mm) are due to the cooling effect of the oxidant stream. Away from the axis, the temperature and the O_2 and CO_2 concentrations are nearly uniform due to the presence of the non-reacting and product-rich external recirculation zone.

At the second station the reaction zone is slightly wider than at the first station due to the expansion of the central jet. The temperature in the central core of the flame has increased due to fuel consumption, while its profile has become flatter due to increased mixing. Despite the low UHC concentration at this station, the CO concentration is still high, which suggests that the conversion of CO to CO_2 is relatively slow.

Further downstream the O_2 and CO_2 concentration profiles progressively flatten as the jet spreads and the CO concentration diminishes due to conversion to CO_2. It is also evident that with increasing distance from the burner, in addition to mixing, thermal radiation also contributes to flattening the temperature profiles.

The predicted results presented in *Figures 5 and 6* were obtained using two different non-uniform grids, one with 59 × 39 and the other with 110 × 81 grid nodes. The two soot

* A stable flame is here defined as one which is lit back, that is, initiated at or very near to the burner (quarl inlet), in contrast to a lifted flame, which may stabilize several burner diameters downstream

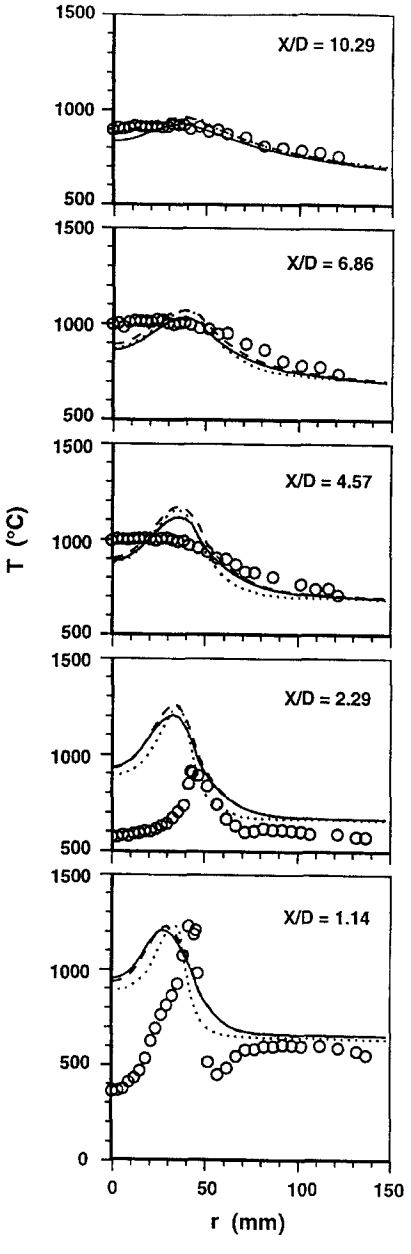

Figure 5 Measured and predicted radial temperature profiles for flame B1. Symbols, measurements; ———, 59 × 39 grid, soot model of Khan *et al.*; – – –, 59 × 39 grid, soot model of Moss *et al.*; ···, 110 × 81 grid, soot model of Khan *et al.*

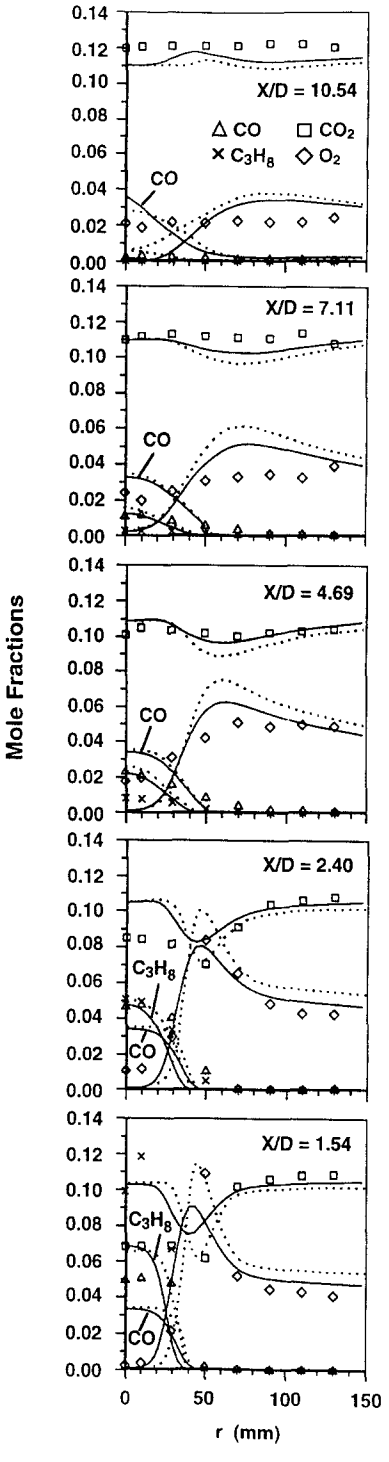

Figure 6 Measured and predicted radial mole fraction profiles (dry basis) for flame B1. Symbols, measurements; ———, coarse grid predictions; – – –, fine grid predictions

formation models mentioned above were used for the calculations carried out using the coarser grid.

At the first station, the model significantly overestimates the temperature at the flame axis and, although it predicts a peak close to that of the measured temperature, it is also unable to reproduce the steep decrease in temperature beyond the flame front. These discrepancies are related to those observed in the species concentrations. The fuel and the CO concentrations were underestimated and the CO_2 concentration was overpredicted at the flame axis, showing that the model predicts a faster fuel consumption rate, which explains the higher predicted temperature. The predicted decay of O_2 and rise in CO_2 concentration beyond the flame front are in close agreement with the measurements.

At $x/D = 2.29$ the predicted and measured temperature profiles are qualitatively similar, but the measured temperatures are lower, especially within the flame region. The predicted shape, with a peak at the flame front, remains up to the last station shown in *Figure 5*, i.e. mixing is slower than in the measurements. Fuel consumption, which was initially overestimated, is underestimated further downstream. The predicted CO concentration changes very slowly along the axial direction, contrary to the measurements. However, the difficulty in the prediction of CO is a well-known shortcoming of the chemical equilibrium assumption.

Figure 5 also shows that the soot formation model has only a marginal influence on the predicted temperature profiles. Its influence on the species concentrations is

negligible. Therefore, the results obtained using the model of Khan and Greeves are not plotted in *Figure 6*, since they are indistinguishable from those computed using the model of Moss and co-workers. The coarseness of the grid has a greater influence on the results, especially close to the burner, where higher temperature and species concentrations gradients are present. Nevertheless, the main features of the predictions and the discrepancies reported above still remain. Therefore, in the following only the results computed using the finer grid and the soot formation model of Khan and Greeves are shown.

To investigate possible reasons for the observed discrepancies, calculations were repeated assuming a linear tangential velocity profile at the inlet, increasing radially, rather than a uniform profile as in the standard calculations. This was motivated by the calculations of Dong and Lilley[28], which show that the inlet flow boundary conditions are extremely important in the simulation of confined swirling flows. It was found that although the temperature profiles slightly changed, the overall behaviour was only marginally affected.

The combustion model has yielded good predictions for other free and confined non-swirling propane flames[16,29]. Therefore, the most probable reason for the observed discrepancies between measurements and predictions seems to lie in the turbulence model. Three different modifications of the standard turbulence model for swirling flows were tried. No improvement was obtained either with the model of Abujelara and Lilley[10] based on the modification of constants C_μ, C_2 and σ_ε of the standard k–ε turbulence model or with the model of Chang and Chen[11] consisting in a hybrid modification to the C_2 constant based on the concept that the modification of anisotropic effects should not be made in the flow regions inherent to small streamline curvatures. The modification of Launder *et al.*[9] consisting in a reduction of the constant C_2 as a function of a gradient Richardson number yielded only marginal improvements, provided that the constant C_2 was not allowed to fall below 90% of its standard value. Therefore, as in other swirling isothermal or reactive flows, these modifications are not universal and thus the minimum order of closure is the algebraic or Reynolds stress model.

Figure 7 shows the radial profiles of predicted NO_x mole fraction together with the measurements for flame B1. High values of NO_x concentration are measured within the flame region at the two stations nearest the burner exit. However, this concentration rapidly decreases in the axial direction and almost uniform values in the range 35–40 ppm occur further downstream. The predictions obtained for the two different values of the constant C given before exhibit similar trends, with higher concentrations predicted using the higher value of C, as expected. Although the predicted NO_x concentration reproduces the measured trends, it underestimates the high values measured close to the centreline, at the first station, and the decrease in NO_x concentration along the axial direction is slower than that measured. Moreover, the NO_x concentration is consistently overpredicted on the lean side of the flame front. The differences observed between the computed NO_x profiles and the data are a consequence both of the temperature and concentration discrepancies and of the NO_x formation model.

It is known that thermal NO_x is maximized near stoichiometric flame zones[6]. However, this is not the case in the profiles shown in *Figure 7*. In addition, because

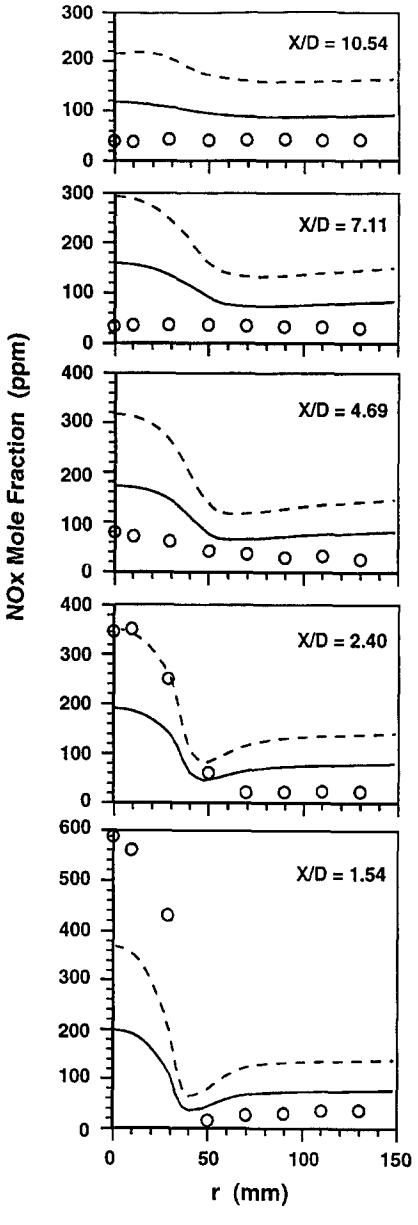

Figure 7 Measured and predicted radial NO_x mole fraction profiles for flame B1. Symbols, measurements; ———, predictions for $C = 6.4 \times 10^6\ s^{-1}$; – – –, predictions for $C = 1.2 \times 10^7\ s^{-1}$

thermal-NO_x formation is strongly temperature-dependent due to its high activation energy, thermal NO_x is significant only at temperatures > 1500°C[30]. The maximum temperature measured for flame B1 barely exceeds 1200°C. Owing to turbulent fluctuations the instantaneous temperature may be sufficiently high to promote thermal-NO_x formation, but the value of the maximum mean temperature reveals that the probability of an instantaneous temperature > 1500°C is small. Hence it is concluded that thermal NO_x does not play an important role in the formation of NO_x in this flame. This conclusion is supported by the mathematical model, which predicts a very small contribution from the thermal route to the total NO_x formed.

The formation of prompt NO_x depends weakly on the temperature, due to the low activation energy in Equation (3). This equation shows that prompt NO_x is proportional to the fuel concentration, which decreases within the flame region in the axial direction as combustion takes place.

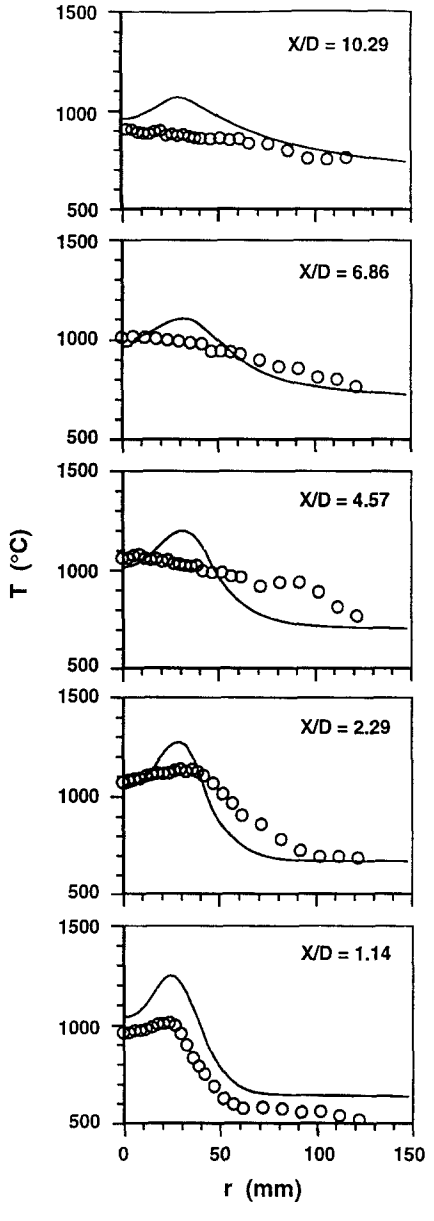

Figure 8 Measured and predicted radial temperature profiles for flame B6. Symbols, measurements; ———, predictions

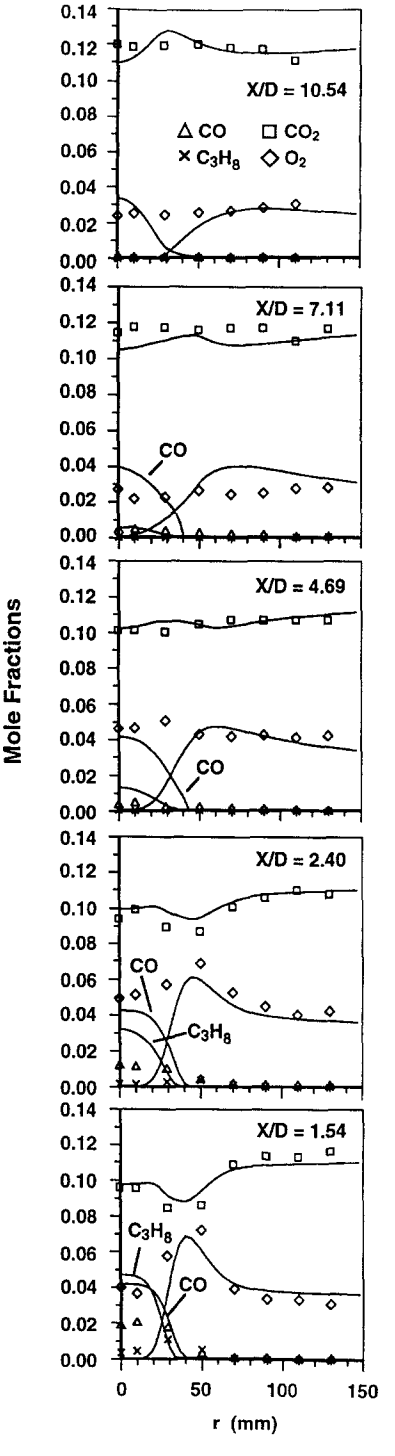

Figure 9 Measured and predicted radial mole fraction profiles (dry basis) for flame B6. Symbols, measurements; ———, predictions

Therefore, the predicted slower decrease of NO_x in the axial direction than in the measurements may be explained by the predicted slower decrease in fuel already reported. Hence, the predicted evolution of NO_x mole fraction can be interpreted in the light of Equation (3).

The results obtained for flame B6 (with FGR) are illustrated in *Figures 8* and *9*. They show that at the first station, the measured temperature at the centreline is higher and the fuel concentration is lower than those for flame B1. The temperature peak has almost vanished. This is explained by the higher momentum of the oxidant stream, which increases the mixing between the oxidant and the fuel and causes a faster fuel consumption rate. The oxygen penetrates to the centreline, where its mole fraction is ~0.04, in contrast to flame B1 where the corresponding mole fraction is very small. Further downstream both the species and the temperature profiles become more uniform, as also observed in flame B1.

Comparison between the predictions and the measurements for flame B6 shows discrepancies similar to those encountered for flame B1. The temperature profile exhibits a peak at the flame front which prevails up to the last station shown, revealing a slower mixing process than that of the measurements. The decrease of fuel concentration along the centreline is underestimated. As stated above, it is believed that the shortcomings of the turbulence model are the main cause of this behaviour.

Figure 10 shows radial profiles of predicted and measured NO_x mole fraction for flame B6. Both the predicted and measured NO_x mole fractions are much smaller for this flame than for flame B1. The high values

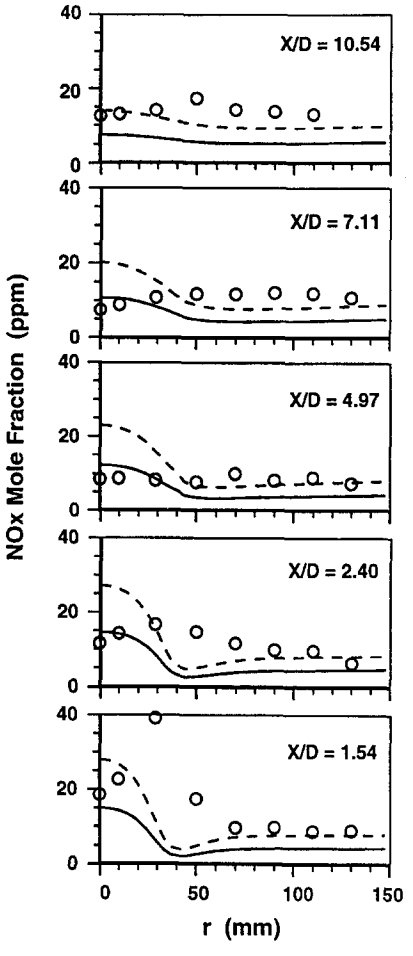

Figure 10 Measured and predicted radial NO_x mole fraction profiles for flame B6. Symbols, measurements; ———, predictions for $C = 6.4 \times 10^6\ s^{-1}$; – – –, predictions for $C = 1.2 \times 10^7\ s^{-1}$

observed for flame B1 near the burner and within the flame region are not present here. The NO_x emission for flame B6 is ~18 ppm, while it was in the range 35–40 ppm for flame B1, both values standardized to 0% O_2 in the combustion products. This is consistent with the lower NO_x concentrations throughout flame B6 brought about by the FGR as observed in *Figure 10*.

The temperatures in the near-burner region are generally well below 1500°C for both flames B1 and B6, undoubtedly due to the high radiation losses. *Figures 5* and *8* show that flame B1 exhibits a higher temperature peak than flame B6. *Figure 6* reveals that for flame B1 this peak occurs near the oxygen-rich oxidant stream. This promotes thermal-NO_x formation in flame B1, in contrast to flame B6 where the maximum flame temperature (see *Figure 8*) occurs in a region of lower O_2 concentrations (see *Figure 9*).

However, as mentioned above, the significant differences in the in-flame NO_x concentrations between flames B1 and B6 are hardly explainable in terms of thermal-NO_x formation because of the relatively low measured temperatures. This implies that prompt NO_x should be an important contributor to the total NO_x concentrations measured for flame B1. The significantly higher UHC concentration observed for flame B1, which indicates a slower burning rate for this flame, favours prompt-NO_x formation. In conclusion, flame B1 has higher total in-flame NO_x concentrations than flame B6 due to both higher thermal- and prompt-NO_x formation.

CONCLUSIONS

The main conclusions to be drawn from this work are the following:

(1) The flue gas data indicate a marked decrease in NO_x emissions with FGR, without significant effects on CO emissions and overall combustion efficiency. At low excess air, UHC emissions significantly decrease on increasing the FGR rate to a value beyond which a further increase in the recirculation rate leaves UHC unchanged.

(2) The present flow configuration produces stable combustion when flue gas is recycled, up to an FGR rate of ~32% regardless of the excess air level in the range studied. The transition between a yellow and a blue flame tends to occur at higher values of R as the excess air increases.

(3) The detailed experimental data for the two flames suggest that the prompt NO_x is an important mechanism of NO formation for the present flow configuration without FGR and that FGR is an effective method of reducing it.

(4) Calculations performed for the two flames confirm the important role of prompt NO_x and the effectiveness of FGR in the reduction of NO_x emissions. However, the comparison between the predicted and the measured temperature and species concentrations, including NO_x, has shown discrepancies, especially close to the burner. It is believed that this is mainly due to the inability of the turbulence model to predict accurately the present confined swirling flames, suggesting that a second-order closure is needed.

ACKNOWLEDGEMENTS

Financial support for this work was partly provided by the European Commission, DG XII (JOULE Programme) and is acknowledged with gratitude. The authors wish also to thank research student Marcos Ruão and technicians Vasco Fred and Manuel Pratas for their valuable contributions to the experiments, and are grateful for the cooperation of Rita Maia and Jorge Coelho during the preparation of the manuscript and figures.

REFERENCES

1 Godridge, A. M., *Journal of the Institute of Energy*, 1988, **61**, 38.
2 Moorman, R. J. and Long, C. H., ASME Paper No. 73-Pwr-21, 1973.
3 Pletnev, G. P., Parchevskii, V. M. and Kolpakov, M. D., *Thermal Engineering*, 1985, **32**, 152.
4 Sigal, I. Ya., Kosinov, O. I., Duboshii, A. N. and Nizhnik, S. S., *Thermal Engineering*, 1986, **33**, 353.
5 Dreher, H., Gass, J., Schuler, O. and Suter, P., in *Second International Conference on Combustion Technologies for a Clean Environment*. Lisbon, 1993.
6 Drake, M. C., Correa, S. M., Pitz, R. W., Shyy, W. and Fenimore, C. P., *Combustion and Flame*, 1987, **69**, 347.
7 De, D. S., *Journal of the Institute of Energy*, 1981, **54**, 113.
8 Sloan, D. G., Smith, P. J. and Smoot, L. D., *Progress in Energy and Combustion Science*, 1986, **12**, 163.

9 Launder, B. E., Priddin, C. H. and Sharma, B. I., *Journal of Fluids Engineering*, 1977, **99**, 231.
10 Abujelara, M. T. and Lilley, D. G., *Chemical Engineering Communications*, 1984, **31**, 223.
11 Chang, K. C. and Chen, C. S., *International Journal of Numerical Methods in Fluids*, 1993, **16**, 421.
12 Gordon, S. and McBride, B. V., *Computer Program for Calculation of Complex Chemical Equilibrium Compositions, Rocket Performance, Incident and Reflected Shocks and Chapman–Jouget Detonations*. NASA SP-273, 1971.
13 Jeng, S. M., Chen, L. D. and Faeth, G. M., in *Nineteenth Symposium (International) on Combustion*. The Combustion Institute, Pittsburgh, 1982, p. 349.
14 Fiveland, W. A., ASME Paper No. 82-HT-20, 1982.
15 Chai, J. C., Lee, H. S. and Patankar, S. V., in *Radiative Heat Transfer: Theory and Applications*, HTD-Vol. 244. ASME, New York, 1993, p. 49.
16 Coelho, P. J. and Carvalho, M. G., *AIAA Journal of Thermophysics and Heat Transfer*, 1995, **9**, 644.
17 Khan, J. M. and Greeves, G., in *Heat Transfer in Flames*, ed. N. H. Afgan and J. M. Beér. Scripta Book Co., 1974, Chapter 25.
18 Syed, K. J., Stewart, C. D. and Moss, J. B., in *Twenty-third Symposium (International) on Combustion*. The Combustion Institute, Pittsburgh, 1990, p. 1533.
19 Stewart, C. D., Syed, K. J. and Moss, J. B., *Combustion Science and Technology*, 1991, **75**, 211.
20 Magnussen, B. F. and Hjertager, B. M., in *Sixteenth Symposium (International) on Combustion*. The Combustion Institute, Pittsburgh, 1977, p. 719.
21 Fenimore, C. P., in *Thirteenth Symposium (International) on Combustion*. The Combustion Institute, Pittsburgh, 1971, p. 373.
22 Fenimore, C. P., *Combustion and Flame*, 1972, **19**, 289.
23 Hayhurst, A. N. and Vince, I. M., *Progress in Energy and Combustion Science*, 1980, **6**, 35.
24 De Soete, G. G., in *Fifteenth Symposium (International) on Combustion*. The Combustion Institute, Pittsburgh, 1974, p. 1093.
25 Warnatz, J., *Chemical Kinetics for Combustion*, Lecture Series (1992)-03. Von Karman Institute for Fluid Dynamics, 1992.
26 Dupont, V., Pourkashanian, M. and Williams, A., *Journal of the Institute of Energy*, 1993, **66**, 20.
27 Weber, R., Peters, A., Breithampt, P. and Visser, B., *Journal of Fluids Engineering*, 1995, **117**, 289.
28 Dong, M. and Lilley, D. G., *Journal of Propulsion and Power*, 1994, **10**, 155.
29 Pereira, J. C. F., Coelho, P. J., Rocha, J. M. P. and Carvalho, M. G., *JSME International Journal, Series B*, 1994, **37**, 659.
30 Nimmo, W., Hampartsoumian, E., Clarke, A. G. and Williams, A., in *Second European Conference of Industrial Furnaces and Boilers*. Algarve, 1991.

NOMENCLATURE

b	reaction order for oxygen
C	constant of the prompt-NO model
D	diameter of secondary air tube
E_a	activation energy
f	factor in the prompt-NO model
f_c	critical value of mixture fraction
fu	fuel
k	reaction rate
M	molecular weight
$\dot{m}$	mass flow rate (kg s^{-1})
r	radial coordinate
R	flue gas recirculation rate (%); molar gas constant
Re	Reynolds number
S	swirl number
t	time
T	temperature
V	axial velocity (m s^{-1})
x	axial distance from quarl exit plane
λ	excess air ratio (actual/stoichiometric air:fuel ratio)
ρ	density

Subscripts

f	fuel
ox	oxidant
pr	prompt
t	thermal